



Spectroelectrochemical Determination of Thiolate Self-Assembled Monolayer Adsorptive Stability in Aqueous and Non-Aqueous Electrolytes

Journal:	<i>Analyst</i>
Manuscript ID	AN-ART-02-2024-000241.R1
Article Type:	Paper
Date Submitted by the Author:	25-Mar-2024
Complete List of Authors:	Siddiqui, Abdur-Rahman; University of Illinois Urbana-Champaign, Chemistry N'Diaye, Jeanne; University of Illinois Urbana-Champaign, Chemistry; University of Illinois Urbana-Champaign Beckman Institute for Advanced Science and Technology Santiago-Carboney, Armando; University of Illinois Urbana-Champaign, Chemistry Martin, Kristin; University of Illinois Urbana-Champaign, Chemistry Bhargava, Rohit; University of Illinois Urbana-Champaign, Bioengineering; University of Illinois Urbana-Champaign Beckman Institute for Advanced Science and Technology Rodriguez-Lopez, Joaquin; University of Illinois Urbana-Champaign, Chemistry; University of Illinois Urbana-Champaign Beckman Institute for Advanced Science and Technology

Spectroelectrochemical Determination of Thiolate Self-Assembled Monolayer Adsorptive Stability in Aqueous and Non-Aqueous Electrolytes

Abdur-Rahman Siddiqui ^{a±}, Jeanne N'Diaye ^{a, b±}, Armando Santiago-Carboney ^{a±}, Kristin

Martin^a, Rohit Bhargava ^{b, c,} and Joaquín Rodríguez-López ^{a, b*}

^a Department of Chemistry, University of Illinois Urbana-Champaign, Urbana, Illinois, 61801, USA

^b The Beckman Institute for Advanced Science and Technology, University of Illinois Urbana-Champaign, Urbana, Illinois 61801, USA

^c Department of Bioengineering, University of Illinois Urbana-Champaign, Urbana, Illinois 61801, United States

±: The authors contributed equally

=

Key Words: self-assembled monolayer, electrochemical stability, non-aqueous, ATR-SEIRAS, SPR, aromatic thiols, adsorption, desorption

Abstract:

Self-assembled monolayers (SAM) are ubiquitous in studies of modified electrodes for sensing, electrocatalysis, and environmental and energy applications. However, determining their adsorptive stability is crucial to ensure robust experiments. In this work, the stable potential window (SPW) in which a SAM-covered electrode can function without inducing SAM desorption were determined for aromatic SAMs on gold electrodes in aqueous and non-aqueous solvents. The SPWs were determined by employing cyclic voltammetry, attenuated total reflectance surface-enhanced infrared absorption spectroscopy (ATR-SEIRAS), and surface plasmon resonance (SPR). The electrochemical and spectroscopic findings concluded that all the aromatic SAMs used displayed similar trends and SPWs. In aqueous systems, the SPW lies between the reductive desorption and oxidative desorption, with pH being the decisive factor affecting the range of the SPW, with the widest SPW observed at pH 1. In the non-aqueous electrolytes, the desorption of SAMs was observed to be slow and progressive. The polarity of the solvent was the main factor in determining the SPW. The lower the polarity of the solvent, the larger the SPW, with 1-butanol displaying the widest SPW. This work showcases the power of spectroelectrochemical analysis and provides ample future directions for the use of non-polar solvents to increase SAM stability in electrochemical applications.

Introduction:

Self-assembled monolayers (SAM) are regarded as a convenient method for functionalizing metal electrode interfaces.¹⁻⁵ Thiols spontaneously adsorb and organize themselves through intermolecular interactions into monolayers on metallic surfaces commonly used in electrochemistry such as Au, Cu, Pt, and others.¹⁻⁵ Due to the ease of preparation and diversity of thiol molecules, thiolate SAMs allow the tailoring of electrode surfaces to many desired properties.¹⁻⁵ Thus, SAM-covered electrodes apply to a plethora of electrochemical applications including electrochemical sensors⁶⁻⁸, electrocatalysis⁹, electrosynthesis^{10,11}, electronic devices^{12,13}, and batteries¹⁴. The use of SAMs in such electrochemical applications requires a fundamental understanding of their adsorptive stability on the electrode, especially when under electrochemical stress. Yet, in the four decades since SAMs were discovered,^{15,16} the long-term adsorptive stability of SAMs remains one of their greatest vulnerabilities.¹⁷⁻¹⁹ The stability of SAMs is correlated to the formation of a high-quality well-packed layer on the electrode surface, with molecules exhibiting strong intermolecular interactions.¹⁷⁻¹⁹ Additionally, the vulnerability of SAMs to various environmental factors such as exposure to high temperatures, light, or air has been thoroughly established.^{17,20-23}

Despite these efforts to understand the factors contributing to SAM stability, there are only a handful of studies focusing on the electrochemical stability of SAMs.²⁴⁻³¹ Ramos et al. established that the electrochemical stability varies by thiol types and pH for different metals, but the quality of the SAM remains the most relevant factor.²⁵ More importantly, they demonstrated that for all electrodes there are discreet potential limits in which a SAM-covered electrode can operate and maintain its integrity.²⁵ This stable

1
2
3 potential window (SPW) is crucial to any electrochemical application utilizing SAMs as
4 the SAM will desorb from the electrode at potentials beyond the SPW. However, these
5 values have only been reported in a few electrolytic systems, primarily in alkaline aqueous
6 electrolytes, as reductive desorption methods in these media have been conveniently
7 used to quantify SAM surface coverage.^{32–34} The anodic limits have been explored
8 sparsely^{34–36}. Thus, expanding the reporting of SPWs of SAMs for a variety of electrolyte
9 environments is an essential analysis that is sorely underrepresented in literature. Such
10 analysis would create convenient guidelines for any electrochemical application that uses
11 SAMs.
12
13
14
15
16
17
18
19
20
21
22
23
24

25 The SPWs of various well-known SAMs were determined utilizing cyclic
26 voltammetry, attenuated total reflectance surface-enhanced infrared absorption
27 spectroscopy (ATR-SEIRAS), and surface plasmon resonance (SPR). Cyclic
28 voltammetry allows a direct assessment of the SAM's electrochemical stability since the
29 SAM passivates the electrode surface inducing solely capacitive anodic and cathodic
30 currents.^{24,37–39} The stability of the SAM can be assessed by maintaining a capacitive
31 current during continuous cycling.^{24,25} In contrast, if the CV profile tends to return to the
32 bare gold baseline, it is taken as an indication that the SAM has desorbed from the
33 electrode surface.^{24,25} Electrochemical SEIRAS (EC-SEIRAS) enables precise
34 monitoring of the SAMs at an electrode interface due to signal enhancement induced by
35 surface plasmon polaritons.^{40,41} Similarly, SPR is a plasmon-driven surface-sensitive
36 measurement that is dependent upon the refractive index of material or solution near the
37 metal surface.⁴² SPR offers the opportunity to measure in situ changes occurring at the
38 gold interface and is easily coupled with electrochemistry.⁴² Therefore, electrochemical-
39
40
41
42
43
44
45
46
47
48
49
50
51
52
53
54
55
56
57
58
59
60

1
2
3 SPR (EC-SPR) can be utilized to probe the stability of SAMs within their respective
4
5 SPWs.⁴³
6
7

8
9 In this work, we expand on the capabilities offered by EC-SEIRAS and EC-SPR to
10 systematically probe SPWs in various electrolytes of interest to the broad
11 electrochemistry community. We report the SPWs of 4 aromatic SAMs in aqueous and
12 non-aqueous solvents on gold electrodes, showing that despite their structural
13 differences, their SPWs remain similar. The aromatic SAMs included 4-mercaptopyridine
14 (4-PySH), 4-mercaptoaniline (4-MA), 4-nitrothiophenol (4-NTP), and 2-
15 mercaptobenzothiazole (2-MBT). 4-PySH was chosen due to its extensive use and
16 characterization in electrochemical literature.^{32,44-47} 4-MA and 4-NTP were utilized due to
17 their similar structure and unique IR signals stemming from their amine⁴⁸⁻⁵⁰ and nitro⁵¹⁻⁵⁵
18 group, respectively. 2-MBT was utilized to act as a control to validate how universal the
19 determined SPWs are for other aromatic SAMs with differing structures, adsorption
20 methods, and surface coverage.⁵⁶⁻⁵⁸ The SPWs were investigated at acidic, neutral, and
21 basic conditions for the aqueous systems. The non-aqueous systems studied were
22 commonly used aprotic solvents and alkyl alcohols.
23
24
25
26
27
28
29
30
31
32
33
34
35
36
37
38
39

40 **Materials and Methods:**

41
42
43 **Chemicals:** All chemicals were purchased from commercial sources and used as
44 received. 4-Mercaptopyridine (95%), 4-mercaptoaniline (97%), 2-mercaptobenzothiazole
45 (97%), potassium hydroxide (KOH, >97%), sodium chloride (NaCl), perchloric acid
46 (HClO₄, 70%), acetonitrile (MeCN, 99%), propylene carbonate (PC, 99%), dimethyl
47 formamide (DMF, 99%), tetrabutylammonium hexafluorophosphate (TBAPF₆, 98%), and
48 gold(III) chloride trihydrate (99.9%) were purchased from Sigma-Aldrich. 4-
49
50
51
52
53
54
55
56
57

1
2
3 nitrothiophenol (96%), methanol (MeOH, 99%), butanol (BuOH, 99%), lithium chloride
4 (LiCl, 99.5%), and sulfuric acid (H₂SO₄, trace metal) were purchased from Thermo Fisher
5 Scientific. Molecules from other suppliers include ethanol (EtOH, 200 proof, Decon Labs),
6 and isopropanol (IPA, 99%, Honeywell). Aqueous solutions were made using deionized
7 water (DI) from a Millipore Sigma Direct-Q 8 (resistivity of 18.2 MΩ).
8
9
10
11
12
13
14
15

16 ***Electrode Preparation and Polishing:*** All electrochemical experiments were performed
17 using a CHI potentiostat (CH Instruments Inc.) with a polycrystalline 2 mm gold working
18 electrode (CH Instruments Inc.), a platinum wire for the counter electrode, and the
19 Ag/AgCl (3 M KCl) reference electrode placed in the cell via a 0.1 M NaClO₄|agar salt
20 bridge. The gold electrode was polished using Buehler MicroCloth polishing pads with 1
21 μm, 0.3 μm, and 0.05 μm alumina suspensions with DI rinse in between. After the last
22 polishing step, the electrode was sonicated for 5 minutes in acetone, IPA, and DI water.
23 A further electrochemical cleaning step was conducted by cycling from 0 V to 1.3 V (vs
24 Ag/AgCl) for 30 cycles in 0.5 M H₂SO₄ at 500 mV/s.
25
26
27
28
29
30
31
32
33
34
35
36
37
38

39 ***Gold Surface Modification and Surface Coverage Calculation:*** All SAMs were formed
40 by submerging the gold electrode in 1 mM solutions of the thiols in EtOH for 10 minutes.
41 Cyclic voltammetry was utilized to assess the surface coverage of the formed thiolate
42 SAMs. Reductive desorption curves (RDC) were performed by cycling between 0 V and
43 -1.3 V in degassed 1M KOH (**Figure S1a**)^{1,32-34}. **Figure S1b** shows the average surface
44 coverage of each SAM calculated using **Equation 1**:
45
46
47
48
49
50
51
52
53

$$\Gamma = Q / nFA \text{ (E1)}$$

54
55
56
57
58
59
60

1
2
3 where Γ is the surface coverage (mol/cm²), Q is the charge (C), n is the number of
4 electrons transferred, F is Faraday's constant (C/mol), and A is the area of the electrode
5 (cm²). The charge was attained by numerical integration of the current described by the
6 RDC.
7
8
9
10
11
12
13
14
15

16 ***Determining the Stable Potential Window (SPW):*** Cyclic voltammograms (CV) were
17 acquired from bare gold electrodes in every solvent tested to act as a baseline to compare
18 against SAM-covered electrodes. Any mention of a baseline is in reference to the CV of
19 a bare gold electrode. The aqueous solvents investigated were 1 M KOH, 0.1 M NaCl,
20 and 0.1 M HClO₄. For the aqueous systems tested: the SAM-covered electrode was
21 cycled from open circuit potential (OCP) negatively until reductive desorption occurred.
22 After another SAM adsorption, the SAM-covered electrode was cycled from OCP
23 positively until oxidative desorption occurred. The non-aqueous solvents investigated
24 were 0.1M TBAPF₆ in MeCN, PC, or DMF, and 0.1 M LiCl in MeOH, EtOH, IPA, or BuOH.
25 For the non-aqueous solvents tested: the SAM-covered electrode was cycled from OCP
26 to increasingly negative potentials in increments of 100 mV. The SAM was determined to
27 have desorbed when the current increased to baseline levels when comparing the same
28 potential window. The same procedure was followed for cycling from OCP to increasingly
29 positive potential. Once the SPWs were established in both aqueous and non-aqueous
30 systems, they were tested with the 4 thiol molecules (4-MA, 4-NTP, 4-PySH, 2-MBT) in
31 each solvent in triplicate. To monitor the integrity of the SAM, the average charge cycled
32 during the cycle was determined by integrating under the anodic sweeps of the triplicate
33 CVs and averaging the attained charge. The average charge and its standard deviation
34
35
36
37
38
39
40
41
42
43
44
45
46
47
48
49
50
51
52
53
54
55
56
57
58
59
60

1
2
3 were plotted versus the cycle number for easier visualization of the continual passivation
4
5 of the electrode due to the SAM on the electrode surface.
6
7

8 ***IR instrumentation and SEIRAS substrate preparation:*** EC-SEIRAS experiments
9
10 were carried out using a Perkin-Elmer Spectrum 3 FTIR with a liquid nitrogen-cooled MCT
11
12 detector. The FTIR was equipped with a VeeMax III (PIKE technologies) specular
13
14 reflection accessory with a Jackfish electrochemical cell (PIKE technologies) for housing
15
16 the specialized low-depth micro-grooved ATR crystal (PIKE technologies) internal
17
18 reflection element (IRE).⁵⁹ The angle of incidence used was 35° with the spectra collected
19
20 between 4000-600 cm⁻¹ at 4 cm⁻¹ resolution using an 8.94 mm J-stop at a scan speed of
21
22 1 cm⁻¹/s. The spectra were taken with an accumulation of 55 scans. The SEIRAS
23
24 substrate was constructed by vacuum depositing 20 nm of gold onto the IRE using a
25
26 Temescal electron-beam evaporator at 0.1 Å/s. The gold-plated IRE was roughened
27
28 following an electrochemical plating of gold islands from our earlier SEIRAS studies.⁶⁰ In
29
30 short using a 10 mM solution of gold (III) chloride trihydrate the potential was pulsed three
31
32 times via chronoamperometry between open circuit potential and -0.35 V with a pulse
33
34 width of 0.25 seconds for 300 steps.
35
36
37
38
39
40

41 ***EC-SEIRAS Verification of SPW:*** All EC-SEIRAS experiments used the gold-plated IRE
42
43 as the working electrode, a carbon rod as the counter electrode, and an Ag/AgCl (3 M)
44
45 as the reference electrode. The corresponding electrolytes were used as background for
46
47 their respective experiments, followed by the modification of the gold-plated IRE with the
48
49 SAMs dissolved in EtOH. After modification, the solution was removed and the EC-
50
51 SEIRAS cell was washed thoroughly with EtOH. The IRE was then purged with Argon to
52
53 eliminate any EtOH contaminates, and the background electrolyte was added back.
54
55
56
57
58
59
60

1
2
3 Potential-dependent spectra were recorded starting at OCP, by holding increasingly
4 negative potentials in increments of 100 mV for 1 minute until the signal from the SAM
5 was lost. After subsequent adsorption of SAMs, the same procedure was followed by
6 holding increasingly positive potentials from OCP.
7
8
9
10
11
12

13 **SPR instrumentation:** All EC-SPR experiments were carried out using a BI-2500 SPR
14 (Biosensing Instrument Inc.) and utilizing commercially available planar (111) gold single
15 crystal sensor chips (Biosensing Instrument Inc.) in a custom-built static EC-SPR cell
16 (**Scheme S1**). The SPR setup is based on the Kretschmann configuration, using a 670
17 nm light source and a detection speed of 4 milliseconds.
18
19
20
21
22
23
24

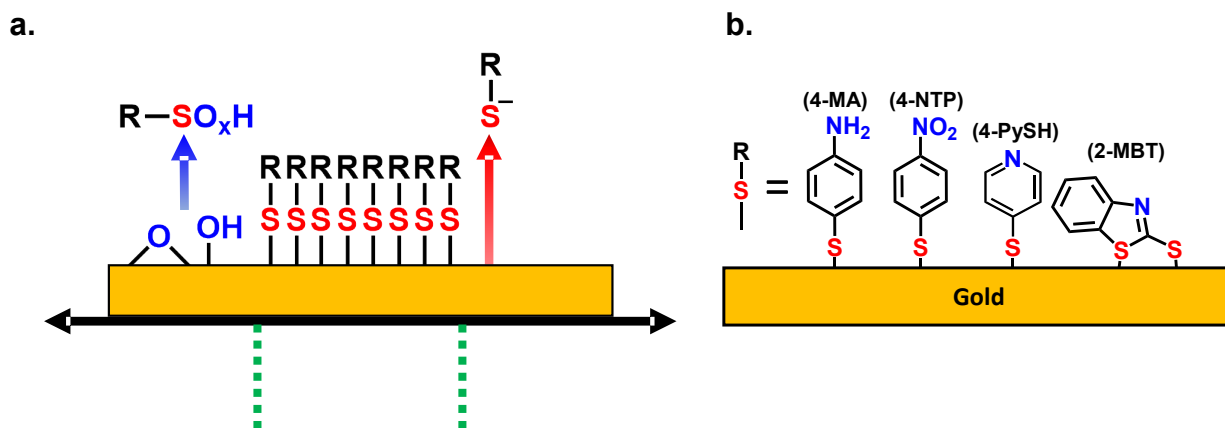
25 **EC-SPR Validation of SPW:** All EC-SPR experiments used the gold sensor chip as the
26 working electrode, a platinum wire as the counter electrode, and an Ag/AgCl (3 M) as the
27 reference electrode. For all SPR experiments, both the bare gold baseline and SAM-
28 modified sensor chips were cycled within the SPWs for a fair comparison. The baseline
29 sensorgrams were obtained in the corresponding electrolytes for each SAM and
30 electrolyte pairing. The gold sensor chip was then modified with SAMs for 15 minutes.
31 The solution was removed, and the cell was rinsed to eliminate any excess electrolyte.
32 Then, beginning at OCP, the systems were cycled within the determined SPWs to monitor
33 refractive index signal shifts. Due to the gold sensor chip being planar(111) and of
34 nanometer thickness, an added level of mindfulness is taken to ensure that Cl⁻ ions did
35 not etch away gold when working with all chloride-based electrolytes.⁶¹
36
37
38
39
40
41
42
43
44
45
46
47
48
49
50

51 **Results and Discussion:**

52 ***Establishing stable potential windows in aqueous systems:***

53
54
55
56
57
58
59
60

The reductive and oxidative desorption of SAMs establishes the two potential limits in which a SAM can remain adsorbed to the gold. Thus, the electrochemical stability of SAMs in aqueous systems is strictly dependent on mitigating these two desorption reactions. **Scheme 1a** depicts the potential range between both desorption reactions as the SPW of the SAMs. **Scheme 1b** displays the 4 different thiol molecules used in the investigation of SPWs.



Scheme 1: (a) Depiction of the stable potential window (SPW) of thiolate SAMs on gold in aqueous solvents. (b) The thiol molecules used to investigate the SPWs: 4-mercaptoaniline (4-MA), 4-nitrothiolphenol (4-NTP), 4-mercaptopyridine (4-PySH), and 2-mercaptobenzothiazole (2-MBT).

Figures 1a-b depict the CVs taken in degassed 1 M KOH with a bare gold electrode and a 4-PySH-covered electrode. When cycling negatively with a bare gold electrode, the CV is solely capacitive until the hydrogen evolution reaction (HER) occurs at potentials beyond -1 V (**Figure 1a**).^{33,35} Conversely, on the cathodic sweep with a SAM-covered electrode, the stripping of the 4-PySH from the electrode surface occurs at approximately -0.5 V.³² The reductive desorption of the SAM is represented in **Equation 2** and **Scheme 1a**, where the Au-S bond cleaves and the SAM desorbs as thiolate species.^{1,32-34} Additional peaks are observed between -0.8 V and -1.1 V, both

corresponding to the desorption of sulfur species on terraces and steps of gold, respectively (**Equation 3**).³²



In contrast, when cycling positively with a bare gold electrode, the anodic sweep comprises the formation of gold oxides (**Equation 4**) at ~ 0.3 V and the oxygen evolution reaction (OER) at 1.1 V (**Figure 1b**).^{35,36} On the returning cathodic sweep, the stripping of the gold oxides can be observed at ~ 0.1 V.^{35,36} When cycling with a SAM-covered electrode, the oxidative desorption (presumably **Equation 5**) and gold oxidation coincide. **Figure 1b** shows the presence of a SAM delays the onset of gold oxidation by 300 mV and the peak current is doubled due to the simultaneous desorption of the SAM and oxidation of gold.^{34–36}

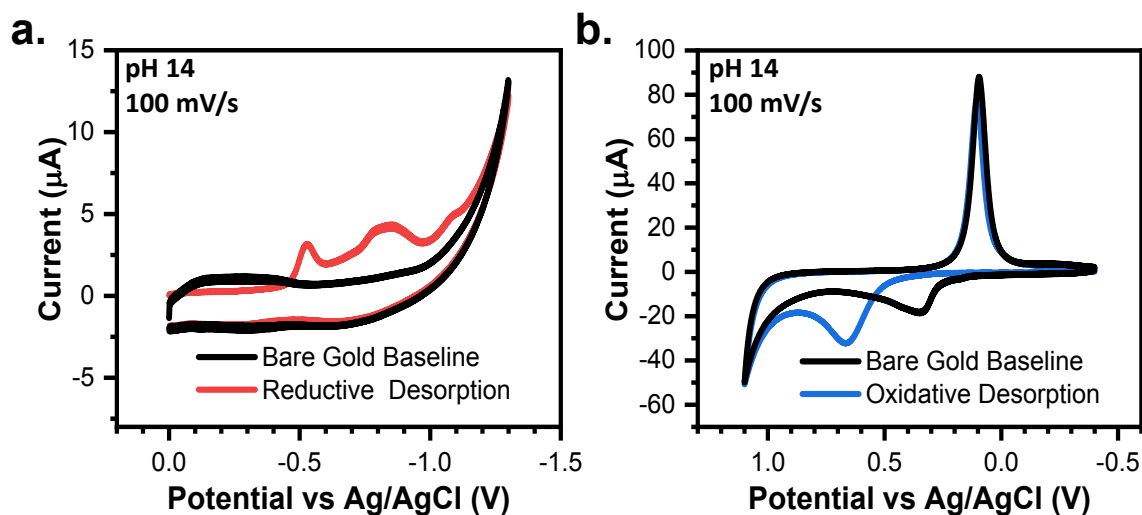
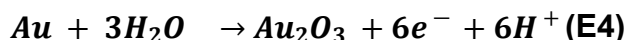


Figure 1: CVs in degassed 1 M KOH showing the (a) reductive desorption and (b) oxidative desorption of 4-PySH compared to baseline bare gold CVs.

Determining the effects of pH on the aqueous stable potential windows:

Figure 2 establishes the SPWs within aqueous systems at different pH values, including alkaline, neutral, and acidic environments. At pH 14, reductive desorption begins to onset at -0.5 V and oxidative desorption occurs at 0.4 V. However, we observed that cycling between these limits leads to an increase in the capacitive current and gold oxidation and stripping are observed, indicating degradation of the SAM (**Figure S2**). Cycling in a narrower window allowed us to identify a more conservative SPW. For example, cycling between 0.3 V and -0.4 V for 50 cycles showed no changes in the voltametric response, thus defining the viable SPW (**Figure 2a**).

Gold oxidation and oxidative desorption are both proton-coupled electron transfer (PCET) reactions (**Equations 4 and 5**).^{34–36} Thus as pH decreases, the onset potentials of both reactions shift a positive 59 mV per unit of pH.^{25,35,36} The onset of gold oxide formation is ~0.3 V, ~0.6 V, and ~1 V at pH 14, 7, and 1, respectively. (**Figures 2a-c**).^{25,36} Thus, in aqueous systems as the pH lowers, the anodic limit of the SPW expands into more positive potentials.²⁵ Conversely, the reductive desorption is pH-independent except when the pH < pKa of the SAM.^{25,34} The pKa of the SAMs used in this study are reported in **Table S1**. For every SAM the reductive desorption of the SAMs is pH-independent and pH-dependent at pH 14 and pH 1, respectively. Thus, as the pH lowers the reductive desorption will shift positively 59 mV/pH. This effectively shortens the reductive limit of the SPW to -0.1 V, -0.2 V, and -0.4 V at pH 1, 7, and 14, respectively (**Figures 2a-c**). Moreover, other PCET reactions such as the oxygen reduction reaction (ORR) and HER, disrupt SAM stability.^{25,34} Thus, the SPW is 800 mV at pH 7 (-0.2 V to 0.6 V) and 1100 mV at pH 1 (1 V to -0.1 V) (**Figures 2b-c**).

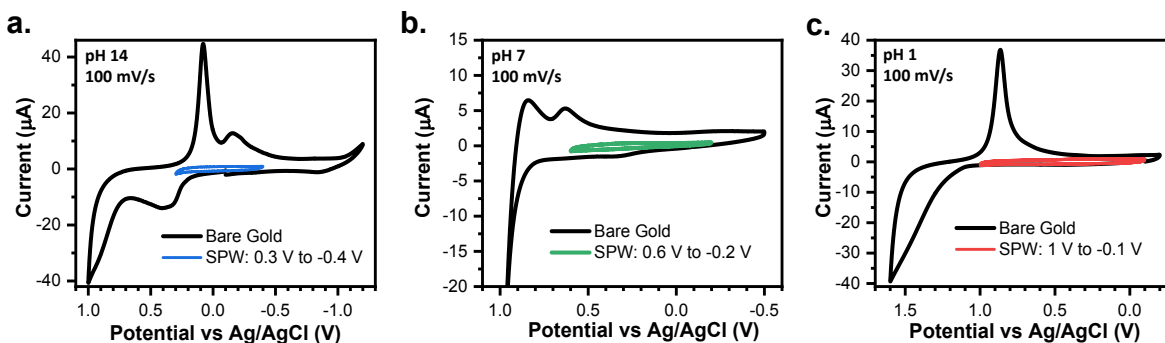


Figure 2: CVs of a bare gold electrode compared to a 4-PySH-covered electrode cycled within the SPW in (a) 1 M KOH (pH 14), (b) 0.1 M NaCl (pH 7), and (c) 0.1 M HClO₄ (pH 1).

Electrochemical assessment of the aqueous stable potential windows:

To verify if the SPW is universal to all SAMs tested, 4-MA, 4-NTP, 4-PySH, and 2-MBT covered electrodes were cycled within the SPWs identified at pH 14, 7, and 1 for 50 cycles in triplicate (**Figure 3**). The SAM-covered electrodes were compared to that of the gold baseline cycled within SPW for a clear demonstration of SAM stability.^{24,37} Remarkably, for every SAM at the studied pHs, the CVs retain their capacitive profile.^{24,37} Since the adsorption of SAMs passivates the electrode surface, with a reduced measured current.^{24,37} The integrity of the SAM can be assessed based on the current levels, however, when the SAM remains intact it is harder to visualize and compare the differences in current strictly based on the capacitive CVs (**Figure 3a-c**). To establish an easier method to monitor the integrity of the SAM, the average charge cycled during the cycle was determined by integrating under the anodic sweeps of the triplicate CVs. The electrochemical stability of the SAMs can be better assessed by plotting the charge from the triplicate CVs versus the cycle number (**Figure 3d-f**). These plots reiterate the consistent electrochemical stability of the SAM within the SPW for every SAM at every pH.^{24,25} Regardless of the SAM, the pH of the solution remains the main factor for the electrochemical stability of these aromatic SAMs.

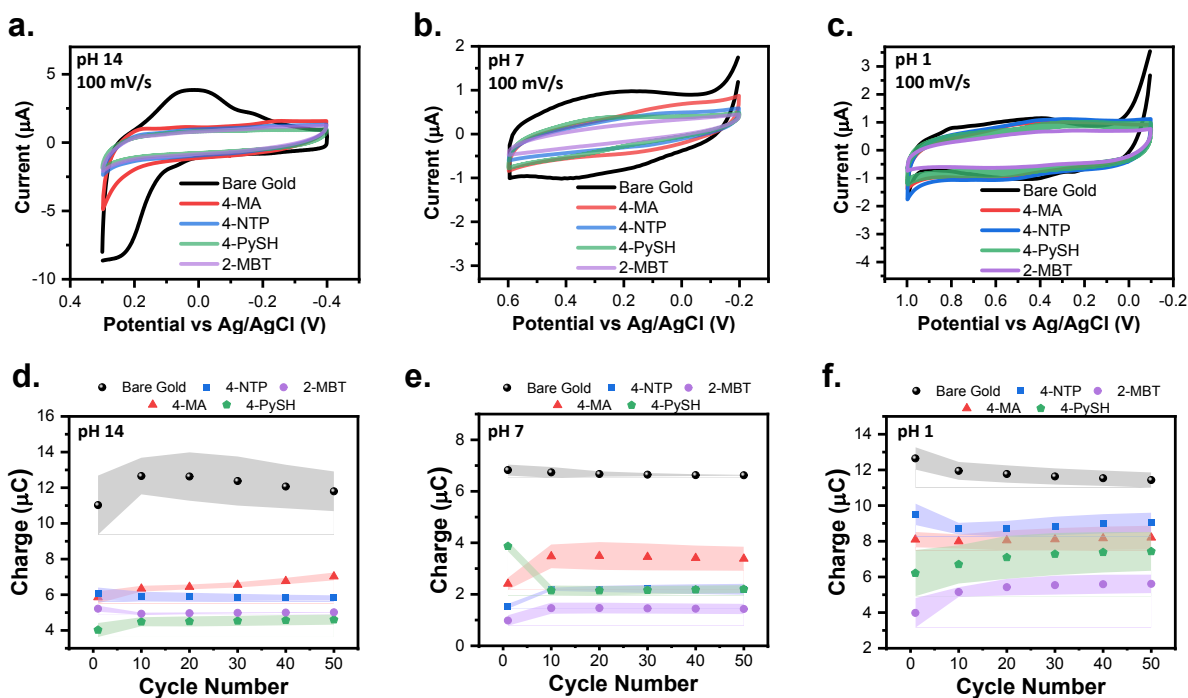


Figure 3: CVs of 4-MA, 4-NTP, 4-PySH, and 2-MBT modified electrodes compared to baseline CVs cycled within the SPWs established for (a) 1 M KOH (pH 14), (b) 0.1 M NaCl (pH 7), and (c) 0.1 M HClO₄ (pH 1). The average integrated charge from the anodic sweeps of the baseline and modified electrodes CVs plotted versus the cycle number in (d) KOH, (e) NaCl, and (f) HClO₄. The shaded regions depict the standard deviation of each measurement for three independent measurements.

Spectroscopic confirmation of the aqueous stable potential windows:

Spectroscopic assessment of the SAM stability was conducted using EC-SEIRAS and EC-SPR to monitor the electrochemical stability of SAMs at interfaces. **Figure 4** shows the potential-dependent spectra obtained for gold-plated IREs modified with 4-NTP at pH 14, 7, and 1. The spectra were acquired while applied potentials were held for 1 minute. The background of the spectra was the spectrum of gold-plated IRE in contact with the electrolyte of interest. Using such a background distinguishes the changes in the IR bands corresponding to the adsorption of 4-NTP and the effect of applied potentials. Negative peaks indicate desorption of the 4-NTP and/or changes in conformation of the

1
2
3 molecules causing vibrational modes to fall outside of selection rules, while positive peaks
4 correlate to the opposite.⁶² The two main peaks observed from 4-NTP correspond to the
5
6 correlate to the opposite.⁶² The two main peaks observed from 4-NTP correspond to the
7
8 asymmetric and symmetrical NO₂ stretches at 1520 cm⁻¹ and 1330 cm⁻¹, respectively.^{63–}
9
10
11
12
13
14
15
16
17
18
19
20
21
22
23
24
25
26
27
28
29
30
31
32
33
34
35
36
37
38
39
40
41
42
43
44
45
46
47
48
49
50
51
52
53
54
55
56
57
58
59
60

Other peaks observed are the aromatic C-C stretching at 1570 cm⁻¹, a C-H twist at 1497 cm⁻¹, and the H-O-H bend at 1650 cm⁻¹.^{51–55} As seen in **Figures 4a-b**, the 4-NTP peaks remain consistent at potentials within the SPW but abruptly disappear when cycled beyond the SPW. However, in acidic conditions at potentials >0.9 V, the 4-NTP signal completely disappears (**Figure 4c**). This is perplexing as CV clearly shows retention of the SAM at these potentials. It is possible that partial degradation of the SAM could lead to structural rearrangement, with the SAM either bending out selection rules at positive potentials⁶² or partially desorbing from the electrode (**Figure S3**).⁶⁶ Moreover, the fast nature of cycling mitigates the desorption of the SAM at potentials where desorption should occur (**Figure S4**). Hence, there is a discrepancy with the potential-dependent spectrum due to holding desorbing potentials for longer amounts of time compared to the CVs. To this point, the IR-based SPWs are more accurate than CV-based SPWs. These spectra confirm and validate the SPWs and the importance of pH on the electrochemical stability of the SAMs.

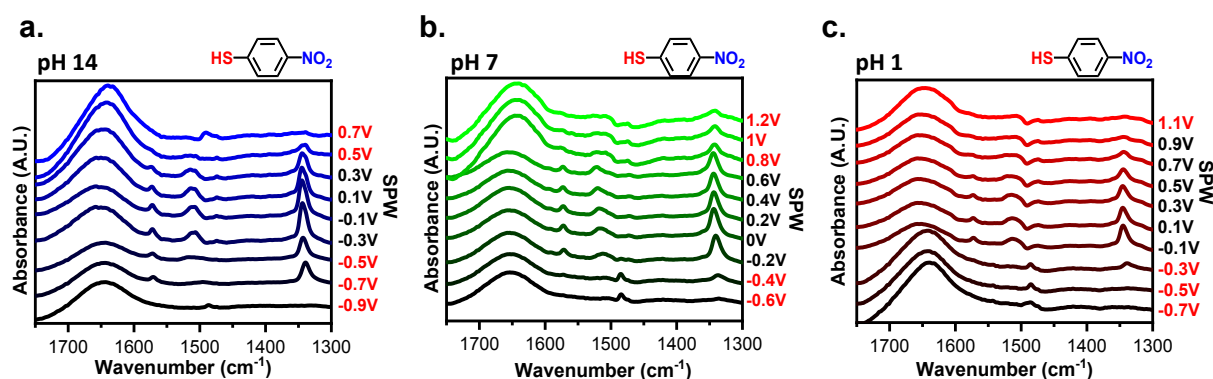


Figure 4: Spectra of a 4-NTP modified gold-plated IRE at different applied potentials

1
2
3 within **(a)** 1 M KOH (pH: 14), **(b)** 0.1 M NaCl (pH: 7), and **(c)** 0.1 M HClO₄ (pH: 1). The
4 potentials marked in red denote those beyond the CV-based SPW.
5
6
7

8 **Figure S5** compares the EC-SPR sensorgrams of a bare gold sensor chip and a
9 4-NTP-covered gold sensor chip at pH 14, 7, and 1 when cycled within their respective
10 SPWs. The sensorgrams exhibit sinusoidal profiles that display the shifts in the refractive
11 index of the gold chip over time as a function of the applied potential.^{42,43} A clear
12 difference between the sensorgrams of the bare and SAM-modified electrodes was
13 observed. The presence of SAMs decreases the magnitude of the shifts in the refractive
14 index, however, the incidence angle increases, a phenomenon that is consistent with the
15 adsorbed species effectively modifying the electrode surface.^{24,42,43} In NaCl electrolyte,
16 the sensorgram of the SAM-covered shows a continual increase in the refractive index
17 which can be attributed to the reported attraction of chlorides to the gold surface (**Figure**
18 **S5b**).⁶¹ These sensorgrams confirm the validity of the SPWs and show the
19 electrochemical stability of the SAMs in aqueous solvents.
20
21
22
23
24
25
26
27
28
29
30
31
32
33
34
35

36 ***Establishing stable potential windows in non-aqueous solvents:***

37
38
39 As established by the results above, the SPW is defined by the cathodic and anodic
40 desorption events. Despite increases in the SPW as the pH decreases, the SPW of
41 aqueous systems are still limited. The ideal system would be a solvent that induces no
42 gold oxides, does not react with the SAM, and hinders the onset of reductive desorption.
43 Aprotic non-aqueous solvents and alcohols seem like good candidates for expanding the
44 SPW beyond those in aqueous systems. For those reasons, the electrochemical stability
45 of thiolate SAMs was assessed in three aprotic solvents and four alcohols. MeCN, PC,
46 and DMF with 0.1M TBAPF₆ supporting electrolyte were assessed due to their abundance
47
48
49
50
51
52
53
54
55
56
57
58
59
60

1
2
3 in the electrochemistry literature.⁶⁷ MeOH, EtOH, IPA, and BuOH with a 0.1M LiCl
4 supporting electrolyte were the four alcohols investigated in this study.
5
6
7
8
9

10 In every case the desorption of the entire SAM did not occur instantly nor at a set
11 potential limit. Instead, a SAM-covered electrode is capable of being cycled over large
12 potential ranges with slow degradation after each cycle (**Figure 5**). The tradeoff to this
13 greater potential range is a decrease in the duration of the electrochemical stability.
14 Because of its larger SPW range, we first discuss the case for 0.1 M LiCl in BuOH. As
15 seen in **Figure 5a**, a baseline was established by cycling between 0.3 V and -1 V. The
16 resulting CV exhibits a capacitive profile with solvent breakdown occurring at negative
17 potentials beyond -0.5 V. Comparing that baseline to the initial cycle of a 4-MA-covered
18 electrode, it is obvious the SAM is passivating the electrode due to lowered anodic and
19 cathodic currents. Yet, with each consecutive cycle, both currents continually increase
20 back to the baseline. This indicates that the SAM is slowly desorbing from the electrode
21 with each passing cycle.²⁵ A similar phenomenon is observed when cycling positively
22 from -0.3 V to 1V (**Figure 5b**). The baseline contains solvent breakdown at potentials
23 greater than 0.7 V. Again, the initial cycle contains lowered currents but after the 25th
24 cycle, the CV of the 4-MA-covered electrode is equivalent to the baseline. Fortunately,
25 there exists an SPW in which the desorption of SAMs can be minimized (**Figure 5c**). The
26 SPWs within non-aqueous solvents differ from those in aqueous systems as there is no
27 clear voltametric desorption in the solvents evaluated. The SPW in non-aqueous solvents
28 is denoted as the potential range in which the electrode remains passivated for at least
29 50 cycles (**Scheme 2**).
30
31
32
33
34
35
36
37
38
39
40
41
42
43
44
45
46
47
48
49
50
51
52
53
54
55
56
57
58
59
60

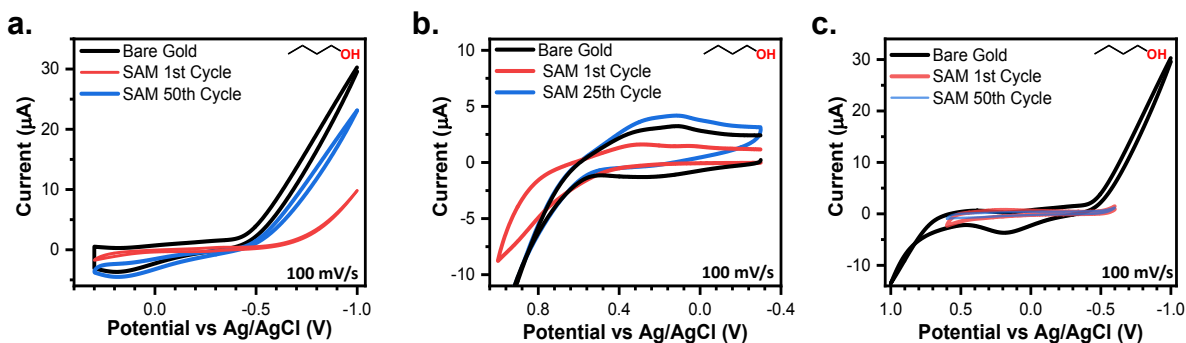
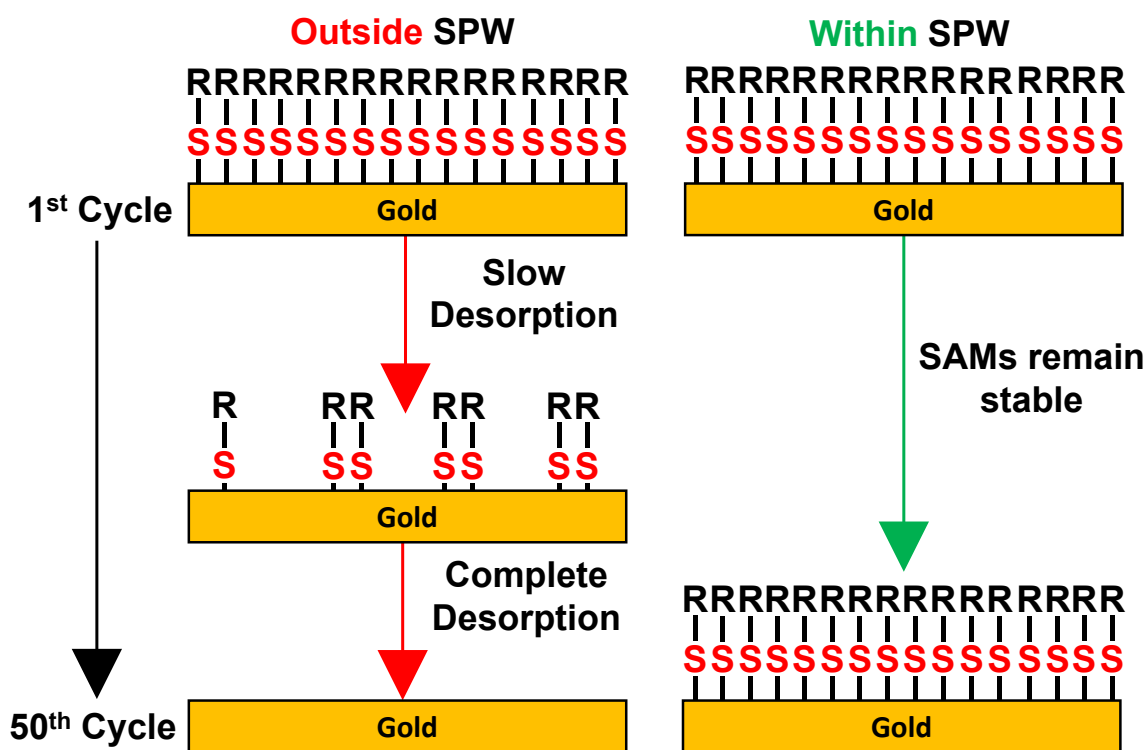


Figure 5: Comparing a baseline CV in 0.1M LiCl BuOH against a 4-MA covered electrode when (a) cycled negatively beyond the SPW and (b) when cycled positively beyond SPW. (c) A scheme of the SPW of thiolate SAMs in non-aqueous solvents.



Scheme 2: Depiction of slow desorption of thiolate SAMs on gold in non-aqueous solvents when cycling to potentials outside the SPW and the retention of the SAM when cycled within the SPW.

Electrochemical assessment of the non-aqueous stable potential windows:

Following the procedure described above, SPWs were identified in the three aprotic solvents (Figure S6) and evaluated based on a consistently passivated CV

1
2
3 compared to the bare gold baseline for 50 cycles. Every aprotic system was assessed in
4
5 triplicate for each SAM following the procedures used for the aqueous systems (**Figure**
6
7 **S7**). The SPW identified were 600 mV in PC (-0.1 V to 0.5 V), 500 mV in DMF (-0.3 V to
8
9 0.2 V), and 400 mV in MeCN (-0.2 V to 0.2 V). For MeCN, PC, and DMF, the initial
10
11 oxidative sweeps contained an oxidation wave consistently larger than any current in the
12
13 baseline (**Figure S7**). For PC and DMF after the initial sweep, the currents lowered and
14
15 remained below the baseline for the remaining 49 cycles (**Figures S7e-f**). For MeCN,
16
17 only a 4-NTP-modified electrode exhibited oxidative current below the baseline for all 50
18
19 cycles (**Figure S7d**). It is apparent long-term electrochemical stability within MeCN is
20
21 inconsistent. It is important to reiterate that modified electrodes in these solvents can still
22
23 operate within large potential windows but only for short durations.
24
25
26
27
28

29 The same procedure used for evaluating the aprotic solvents was used for
30
31 identifying SPWs in the alcohols (**Figure S8**) and evaluating them. The SPWs are
32
33 equivalent for both MeOH and EtOH at 400 mV (-0.2 V to 0.2 V) (**Figures 6a-b**). The
34
35 SPW increases to 900 mV in IPA (-0.6 V to 0.3 V) and further expands to 1200 mV in
36
37 BuOH (-0.6 V to 0.6 V) (**Figure 6c-d**). **Figures 6e-h** show the SAM-covered electrode
38
39 consistently remained passivated for all 50 cycles when cycled within the SPW for every
40
41 alcohol. The only two outliers are the initial cycle of 4-MA and 4-PySH in BuOH, yet the
42
43 current remained below the baseline (**Figures 6h**).
44
45
46
47

48 An interesting trend emerges that the SPW expands with increasing alkyl chain
49
50 length of the alcohols. Just as pH was the main factor for SPWs in aqueous systems, we
51
52 posit that the solubility of the SAM is the main factor in non-aqueous systems. With
53
54 increasing alkyl chain length the alcohol becomes less polar.⁶⁸ The polar SAMs used in
55
56
57
58
59
60

this study are less soluble in non-polar solvents, therefore, due to the sluggish kinetics for dissolution of thiolates in these solvents, the SAMs remain attached to the electrode for larger potential windows. This explanation is confirmed by both the slow desorption of SAMs in non-aqueous systems (**Figure 5**) and by the observation that the SPW increases with decreasing polarity index (**Table S2**).⁶⁸ These observations line up with established literature that thiolate-capped gold nanoparticles remain stable in toluene and hexane which have polarity indexes of 2.4 and 0.1, respectively.^{4,68} Moreover, the electrochemical stability of alkanethiols increases with increasing alkyl chain length.^{1,25} Further conformation is found in the observation that the aprotic solvents used here are the most polar non-aqueous solvents used, while the electrochemical stability of the SAMs is most inconsistent in these solvents (**Figures S7e-f**).

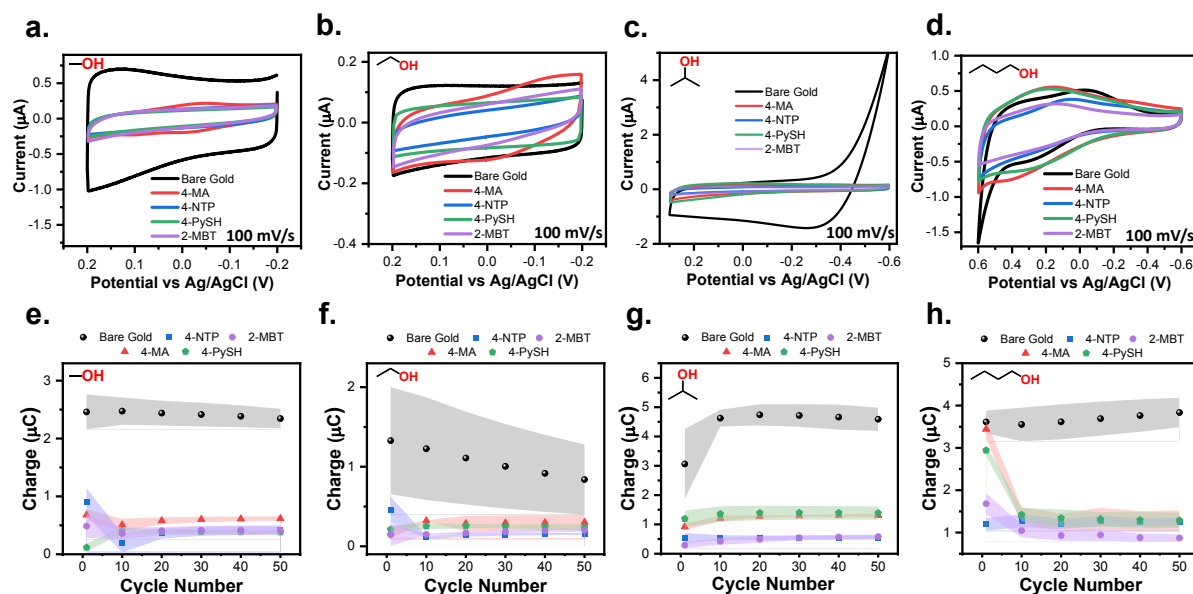


Figure 6: CVs of 4-MA, 4-NTP, 4-PySH, and 2-MBT modified electrodes compared to baseline CVs cycled within the SPWs established for 0.1 M LiCl (**a**) MeOH, (**b**) EtOH, (**c**) IPA, and (**d**) BuOH. The average integrated charge from the anodic sweeps of the baseline and modified electrodes CVs plotted versus the cycle number in (**e**) MeOH, (**f**) EtOH, (**g**) IPA, and (**h**) BuOH. The shaded regions depict the standard deviation of each measurement for three independent measurements.

Spectroelectrochemical validation of non-aqueous stable potential windows:

EC-SEIRAS was used to verify the non-aqueous SPWs and evaluate the slow desorption. Potential-dependent spectra were measured for gold-plated IREs modified with 4-MA. The background of the spectra was the spectrum of gold-plated IRE in contact with the electrolyte being assessed. The two main peaks observed from 4-MA correspond to the C-C stretch of the aryl ring at $\sim 1590\text{ cm}^{-1}$ and the N-H stretch of the amine at 1620 cm^{-1} .^{48–50} In MeCN and PC the 4-MA peaks remain observable even at potentials beyond the CV-based SPW (**Figures S9a-b**). For DMF the 1590 cm^{-1} peak is only observed for positive potential close to the CV-based SPW (**Figure S9c**). These spectra further display the slow desorption in non-aqueous solvents and exemplify the inconsistencies of the SPWs in the polar aprotic electrolytes.

This trend of the 1590 cm^{-1} peak shrinking at negative potentials and growing at positive potentials could be due to either desorption at negative potentials or the SAM bending out of selection rules due to potential-induced conformation changes (**Scheme S2**).⁶⁹ When applying negative potentials, a SAM can undergo a conformation change induced by the permeation of ions into the SAM while at positive potentials these changes are reported to be smaller or not observed.⁶⁹ Thus, conformation changes will only occur at negative potentials and should be reversible when applying positive potentials.⁶⁹ The reversibility of this potential-induced conformation change is best exemplified within BuOH (**Figure S10**), The signal derived from the 4-MA lowers with increasingly negative applied potential. Yet, upon applying positive potential immediately after, the 4-MA signal returns and grows with progressively positive applied potential.

Figure 7 shows the potential-dependent spectra of a 4-MA modified gold-plated IRE in every alcohol. The spectra of the alcohols all display signals from the 1590 cm^{-1} C-C stretch and vary in capacity to resolve the 1620 cm^{-1} N-H stretch. In MeOH, EtOH, and IPA the 4-MA peaks alter significantly even within their voltametric SPW (**Figures 7a-c**). Like the aprotic electrolytes, for potentials within the SPW, the 1590 cm^{-1} peak shrinks at negative potentials and grows at positive potentials. The same explanation of the SAM bending it out of selection rules can apply to these systems as well (**Scheme S2**).⁶⁹ **Figure 7d** confirms SAMs can exist on an electrode cycled in BuOH negatively longer than cycling positively as seen in **Figure 5**. The 4-MA signal slowly diminishes when cycled beyond -0.2 V, but the signal abruptly disappears past 0.4 V.

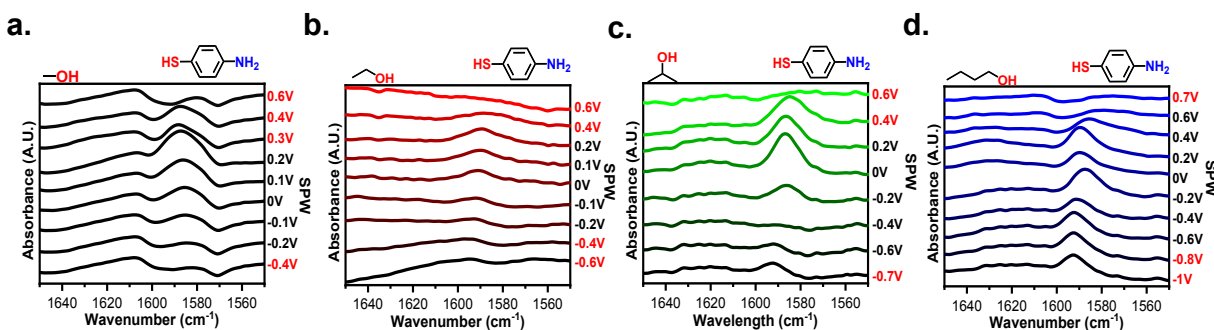
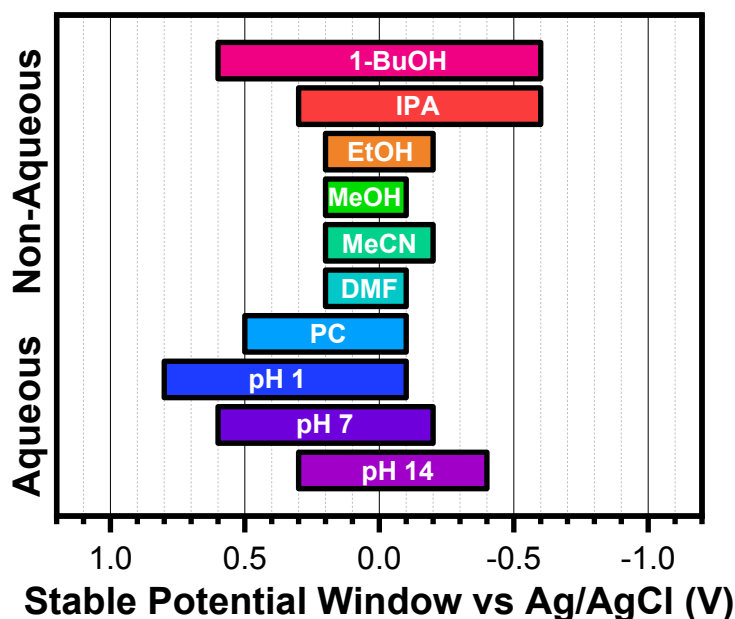


Figure 7: Spectra of a 4-MA modified SEIRAS substrate at different applied potentials within 0.1 M LiCl (**a**) MeOH, (**b**) EtOH (**c**) IPA, and (**d**) BuOH. The voltages marked in red denote applied potentials beyond the CV-based SPW.

EC-SPR was used to further study the spectroscopic interactions of the SAMs in non-aqueous solvents (**Figures S11 and S12**). Both the baseline and 4-MA-covered gold sensor chips were cycled within the SPWs and monitored with the SPR.^{24,42,43} Baseline measurements for the non-aqueous solvents were not possible as the BI-2500 reached detection limits due to their high refractive indexes'. Yet, the 4-MA modified sensor chips were able to obtain SPR signals from the SAM interacting with these solvents while cycling within their respective SPWs. (**Figures S11 and S12a**). The key takeaway is this

1
2
3 signal is observed solely when the SAMs are modifying the surface. Therefore, since this
4
5 signal remains while cycling within the respective SPW in each solvent, the SAMs are
6
7 stable. The sensorgrams of the alcohols demonstrate a sloping profile which is attributed
8
9 to the attraction of the Cl^- ions with the gold surface.⁶¹ MeCN demonstrated a similar
10
11 sensorgram to the alcohols which could be attributed to the adsorption of MeCN onto
12
13 gold. 70,71 There were no clear signals from either DMF or PC (**Figure S12b-c**).

14
15
16
17
18 A summary of these findings is shown in **Scheme 3**. These SPWs have been
19
20 confirmed to work for both types of gold electrodes used in this work (**Figure S13**).
21
22 Interesting future directions could investigate the applicability of these findings with a wide
23
24 variety of SAMs, explore the stability in more non-polar solvents, and study the effects of
25
26 supporting electrolytes on electrochemical stability.
27
28
29



30
31
32
33
34
35
36
37
38
39
40
41
42
43
44
45
46
47
48
49
50
51 **Scheme 3:** Summary of the identified SPWs for aromatic SAMs on gold in each aqueous
52 and non-aqueous solvent investigated.

53
54
55 **Conclusions:**

1
2
3 In this study, we successfully used CV and ATR-SEIRAS to detect changes
4 associated with SAM desorption events on modified gold electrodes. Using these
5 techniques, we determined the stable potential windows of electrodes modified with
6 aromatic SAMs in aqueous electrolytes as a function of pH and non-aqueous electrolytes
7 for selected alcohols and aprotic polar solvents. Our results demonstrate that the SPWs
8 determined universally apply to all four aromatic SAMs in every system tested, thus
9 greatly simplifying our determined results (**Scheme 3**). In aqueous systems, the potential
10 range between the two reductive desorption and oxidative desorption/gold oxidation
11 defined the stable potential window. Clear voltametric features and well-defined changes
12 in the SEIRAS signatures were measured for all cases. The pH was the largest factor for
13 determining the range of the SPW as it directly delayed the onset of oxidative desorption
14 to higher potentials. Since gold oxidation is pH-dependent, the SPW increases with
15 decreasing pH. The largest SPW (1.1 V wide) was observed for pH 1. In the non-aqueous
16 solvents, instead of being limited to potentials between desorption events, SAM slowly
17 dissolves into solution when cycled at large potential ranges. The non-aqueous SPW was
18 defined as the potential range the SAM-covered electrode could be cycled for 50 cycles
19 without degradation of the SAM. It was determined that the polarity of the solvent was the
20 main indicator for the SPW. The lower the polarity index of the solvent, the larger the
21 SPW. The largest SPW (1.2 V wide) was observed for 0.1 M LiCl in 1-butanol. Our
22 findings unambiguously demonstrate that the solvent utilized is the biggest decider in the
23 electrochemical stability of aromatic SAMs. This work opens a new opportunity for further
24 investigations into the uses of non-polar solvents in electrochemical applications involving
25
26
27
28
29
30
31
32
33
34
35
36
37
38
39
40
41
42
43
44
45
46
47
48
49
50
51
52
53
54
55
56
57
58
59
60

1
2
3 SAMs, such as electrosynthesis, catalysis, battery research, and CO₂ capture and
4 conversion, the latter of which our laboratory is exploring using modified electrodes.
5
6
7

8 **Supporting Information:** The SPR data, additional schemes, tables, and experimental
9 results. surface coverages of the SAMs, identification of the SPWs in non-aqueous
10 systems, CVs, and SEIRAS spectra in non-aqueous systems.
11
12
13
14
15

16 **Author Contributions:**

17
18 A.S. and J.N. contributed to conceptualization, investigation, methodology, formal
19 analysis, validation, visualization, writing the original draft, reviewing, and editing. A.S.C
20 and K.M. contributed to formal analysis, investigation, validation, visualization, writing the
21 original draft, and reviewing and editing. R.G. contributed to funding acquisition,
22 resources, reviewing and editing. J.R.L contributed to funding acquisition, resources,
23 supervision, project administration, reviewing and editing.
24
25
26
27
28
29
30
31
32

33 **Conflicts of Interest:** There are no conflicts to declare.
34
35

36 **Acknowledgements:**

37
38 This material is based upon work supported by the U.S. Department of Energy, Office of
39 Science, Office of Basic Energy Sciences, Materials Chemistry program under Award
40 Number DE-SC0022173. This work was carried out in part in the Materials Research
41 Laboratory Central Research Facilities, University of Illinois. J.N. thanks the Arnold and
42 Mabel Beckman Foundation for supporting this work through a Beckman-Brown
43 Postdoctoral Fellowship at the Beckman Institute, University of Illinois at Urbana-
44 Champaign. We acknowledge helpful discussions with Dr. Adolfo I.B. Romo and Dr. Md.
45 Sazzad Hossain about this project.
46
47
48
49
50
51
52
53
54
55
56
57
58
59
60

References:

- (1) Love, J. C.; Estroff, L. A.; Kriebel, J. K.; Nuzzo, R. G.; Whitesides, G. M. Self-Assembled Monolayers of Thiolates on Metals as a Form of Nanotechnology. *Chem. Rev.* **2005**, *105* (4), 1103–1170. <https://doi.org/10.1021/cr0300789>.
- (2) Tverdokhlebova, A.; Sterin, I.; Smutok, O.; Katz, E. Modification of Electrodes with Self-Assembled Monolayers—General Principles. *J. Solid State Electrochem.* **2023**. <https://doi.org/10.1007/s10008-023-05700-w>.
- (3) Ghorbanizamani, F.; Guler Celik, E.; Moulahoum, H.; Timur, S. Chapter 1 - Self-Assembled Monolayer-Based Nanoscaled Surfaces. In *Biophysics At the Nanoscale*; Denizli, A., Ed.; Academic Press, 2024; pp 1–25. <https://doi.org/10.1016/B978-0-443-15359-4.00001-2>.
- (4) Vericat, C.; Vela, M. E.; Benitez, G.; Carro, P.; Salvarezza, R. C. Self-Assembled Monolayers of Thiols and Dithiols on Gold: New Challenges for a Well-Known System. *Chem. Soc. Rev.* **2010**, *39* (5), 1805–1834. <https://doi.org/10.1039/B907301A>.
- (5) Vericat, C.; E. Vela, M.; Corthey, G.; Pensa, E.; Cortés, E.; H. Fonticelli, M.; Ibañez, F.; E. Benitez, G.; Carro, P.; C. Salvarezza, R. Self-Assembled Monolayers of Thiolates on Metals: A Review Article on Sulfur-Metal Chemistry and Surface Structures. *RSC Adv.* **2014**, *4* (53), 27730–27754. <https://doi.org/10.1039/C4RA04659E>.
- (6) Markovic, A.; Buschbeck, L.; Brand, I.; Dosche, C.; Christoffers, J.; Wittstock, G. Electrochemical Activation of Self-Assembled Monolayers for the Binding of Effectors. *Langmuir* **2020**, *36* (48), 14623–14632. <https://doi.org/10.1021/acs.langmuir.0c02426>.
- (7) Mandler, D.; Kraus-Ophir, S. Self-Assembled Monolayers (SAMs) for Electrochemical Sensing. *J. Solid State Electrochem.* **2011**, *15* (7), 1535–1558. <https://doi.org/10.1007/s10008-011-1493-6>.
- (8) Shaver, A.; Curtis, S. D.; Arroyo-Currás, N. Alkanethiol Monolayer End Groups Affect the Long-Term Operational Stability and Signaling of Electrochemical, Aptamer-Based Sensors in Biological Fluids. *ACS Appl. Mater. Interfaces* **2020**, *12* (9), 11214–11223. <https://doi.org/10.1021/acsami.9b22385>.
- (9) Shang, H.; Wallentine, S. K.; Hofmann, D. M.; Zhu, Q.; Murphy, C. J.; Baker, L. R. Effect of Surface Ligands on Gold Nanocatalysts for CO₂ Reduction. *Chem. Sci.* **2020**, *11* (45), 12298–12306. <https://doi.org/10.1039/D0SC05089J>.
- (10) Li, M.; Li, Y. Solid-Phase Electrosynthesis. *Acc. Chem. Res.* **2023**, *56* (24), 3694–3703. <https://doi.org/10.1021/acs.accounts.3c00620>.

- 1
2
3 (11) Heo, J.; Ahn, H.; Won, J.; Son, J. G.; Shon, H. K.; Lee, T. G.; Han, S. W.; Baik, M.-H. Electro-
4 Inductive Effect: Electrodes as Functional Groups with Tunable Electronic Properties.
5 *Science* **2020**, *370* (6513), 214–219. <https://doi.org/10.1126/science.abb6375>.
6
7
8 (12) Singh, M.; Kaur, N.; Comini, E. The Role of Self-Assembled Monolayers in Electronic
9 Devices. *J. Mater. Chem. C* **2020**, *8* (12), 3938–3955. <https://doi.org/10.1039/D0TC00388C>.
10
11 (13) Kim, S.; Yoo, H. Self-Assembled Monolayers: Versatile Uses in Electronic Devices from
12 Gate Dielectrics, Dopants, and Biosensing Linkers. *Micromachines* **2021**, *12* (5), 565.
13 <https://doi.org/10.3390/mi12050565>.
14
15
16 (14) Yi, R.; Mao, Y.; Shen, Y.; Chen, L. Self-Assembled Monolayers for Batteries. *J. Am. Chem.*
17 *Soc.* **2021**, *143* (33), 12897–12912. <https://doi.org/10.1021/jacs.1c04416>.
18
19 (15) Nuzzo, R. G.; Allara, D. L. Adsorption of Bifunctional Organic Disulfides on Gold Surfaces.
20 *J. Am. Chem. Soc.* **1983**, *105* (13), 4481–4483. <https://doi.org/10.1021/ja00351a063>.
21
22
23 (16) Strong, L.; Whitesides, G. M. Structures of Self-Assembled Monolayer Films of
24 Organosulfur Compounds Adsorbed on Gold Single Crystals: Electron Diffraction Studies.
25 *Langmuir* **1988**, *4* (3), 546–558. <https://doi.org/10.1021/la00081a009>.
26
27 (17) Srisombat, L.; Jamison, A. C.; Lee, T. R. Stability: A Key Issue for Self-Assembled
28 Monolayers on Gold as Thin-Film Coatings and Nanoparticle Protectants. *Colloids Surf.*
29 *Physicochem. Eng. Asp.* **2011**, *390* (1–3), 1–19.
30 <https://doi.org/10.1016/j.colsurfa.2011.09.020>.
31
32
33 (18) Chen, N.; Li, S.; Zhao, P.; Liu, R.; Xie, Y.; Lin, J.-L.; Nijhuis, C. A.; Xu, B.; Zhang, L.; Xu, H.; Li,
34 Y. Extreme Long-Lifetime Self-Assembled Monolayer for Air-Stable Molecular Junctions. *Sci.*
35 *Adv.* **2023**, *9* (42), eadh3412. <https://doi.org/10.1126/sciadv.adh3412>.
36
37
38 (19) Yu, T.; Marquez, M. D.; Tran, H.-V.; Lee, T. R. Crosslinked Organosulfur-Based Self-
39 Assembled Monolayers: Formation and Applications. *Soft Sci.* **2022**, *2* (2).
40 <https://doi.org/10.20517/ss.2022.04>.
41
42
43 (20) Schlenoff, J. B.; Li, M.; Ly, H. Stability and Self-Exchange in Alkanethiol Monolayers. *J.*
44 *Am. Chem. Soc.* **1995**, *117* (50), 12528–12536. <https://doi.org/10.1021/ja00155a016>.
45
46 (21) Asyuda, A.; Das, S.; Zharnikov, M. Thermal Stability of Alkanethiolate and Aromatic
47 Thiolate Self-Assembled Monolayers on Au(111): An X-Ray Photoelectron Spectroscopy
48 Study. *J. Phys. Chem. C* **2021**, *125* (39), 21754–21763.
49 <https://doi.org/10.1021/acs.jpcc.1c06984>.
50
51
52 (22) Schoenfish, M. H.; Pemberton, J. E. Air Stability of Alkanethiol Self-Assembled
53 Monolayers on Silver and Gold Surfaces. *J. Am. Chem. Soc.* **1998**, *120* (18), 4502–4513.
54 <https://doi.org/10.1021/ja974301t>.
55
56
57
58
59
60

- 1
2
3 (23) Cortés, E.; Rubert, A. A.; Benitez, G.; Carro, P.; Vela, M. E.; Salvarezza, R. C. Enhanced
4 Stability of Thiolate Self-Assembled Monolayers (SAMs) on Nanostructured Gold Substrates.
5 *Langmuir* **2009**, *25* (10), 5661–5666. <https://doi.org/10.1021/la804251a>.
6
7
8 (24) Beulen, M. W. J.; Kastenbergh, M. I.; van Veggel, F. C. J. M.; Reinhoudt, D. N.
9 Electrochemical Stability of Self-Assembled Monolayers on Gold. *Langmuir* **1998**, *14* (26),
10 7463–7467. <https://doi.org/10.1021/la981031z>.
11
12
13 (25) Ramos, N. C.; Medlin, J. W.; Holewinski, A. Electrochemical Stability of Thiolate Self-
14 Assembled Monolayers on Au, Pt, and Cu. *ACS Appl. Mater. Interfaces* **2023**, *15* (11),
15 14470–14480. <https://doi.org/10.1021/acsami.3c01224>.
16
17
18 (26) Hakamada, M.; Takahashi, M.; Furukawa, T.; Tajima, K.; Yoshimura, K.; Chino, Y.;
19 Mabuchi, M. Electrochemical Stability of Self-Assembled Monolayers on Nanoporous Au.
20 *Phys. Chem. Chem. Phys.* **2011**, *13* (26), 12277–12284.
21 <https://doi.org/10.1039/C0CP02553D>.
22
23
24 (27) Kolodziej, A.; Fernandez-Trillo, F.; Rodriguez, P. Determining the Parameters Governing
25 the Electrochemical Stability of Thiols and Disulfides Self-Assembled Monolayer on Gold
26 Electrodes in Physiological Medium. *J. Electroanal. Chem.* **2018**, *819*, 51–57.
27 <https://doi.org/10.1016/j.jelechem.2017.07.039>.
28
29
30 (28) Salvarezza, R. C.; Carro, P. The Electrochemical Stability of Thiols on Gold Surfaces. *J.*
31 *Electroanal. Chem.* **2018**, *819*, 234–239. <https://doi.org/10.1016/j.jelechem.2017.10.046>.
32
33
34 (29) Thom, I.; Buck, M. Electrochemical Stability of Self-Assembled Monolayers of Biphenyl
35 Based Thiols Studied by Cyclic Voltammetry and Second Harmonic Generation. *Surf. Sci.*
36 **2005**, *581* (1), 33–46. <https://doi.org/10.1016/j.susc.2005.02.029>.
37
38
39 (30) Li, J.; Shen, Y.; Zhang, Y.; Liu, Y. Room-Temperature Ionic Liquids as Media to Enhance
40 the Electrochemical Stability of Self-Assembled Monolayers of Alkanethiols on Gold
41 Electrodes. *Chem. Commun.* **2005**, No. 3, 360–362. <https://doi.org/10.1039/B412412J>.
42
43
44 (31) Badgurjar, D.; Huynh, M.; Masters, B.; Wuttig, A. Non-Covalent Interactions Mimic the
45 Covalent: An Electrode-Orthogonal Self-Assembled Layer. *J. Am. Chem. Soc.* **2023**, *145* (32),
46 17734–17745. <https://doi.org/10.1021/jacs.3c04387>.
47
48
49 (32) Ramírez, E. A.; Cortés, E.; Rubert, A. A.; Carro, P.; Benítez, G.; Vela, M. E.; Salvarezza, R.
50 C. Complex Surface Chemistry of 4-Mercaptopyridine Self-Assembled Monolayers on
51 Au(111). *Langmuir* **2012**, *28* (17), 6839–6847. <https://doi.org/10.1021/la204951u>.
52
53
54 (33) Walczak, M. M.; Popenoe, D. D.; Deinhammer, R. S.; Lamp, B. D.; Chung, C.; Porter, M. D.
55 Reductive Desorption of Alkanethiolate Monolayers at Gold: A Measure of Surface
56 Coverage. *Langmuir* **1991**, *7* (11), 2687–2693. <https://doi.org/10.1021/la00059a048>.
57
58
59
60

- 1
2
3 (34) Widrig, C. A.; Chung, C.; Porter, M. D. The Electrochemical Desorption of N-Alkanethiol
4 Monolayers from Polycrystalline Au and Ag Electrodes. *J. Electroanal. Chem. Interfacial*
5 *Electrochem.* **1991**, *310* (1), 335–359. [https://doi.org/10.1016/0022-0728\(91\)85271-P](https://doi.org/10.1016/0022-0728(91)85271-P).
6
7
8 (35) Burke, L. D.; Nugent, P. F. The Electrochemistry of Gold: I the Redox Behaviour of the
9 Metal in Aqueous Media. *Gold Bull.* **1997**, *30* (2), 43–53.
10 <https://doi.org/10.1007/BF03214756>.
11
12 (36) Yang, S.; Hettler, D. G. H. Redefinition of the Active Species and the Mechanism of
13 the Oxygen Evolution Reaction on Gold Oxide. *ACS Catal.* **2020**, *10* (21), 12582–12589.
14 <https://doi.org/10.1021/acscatal.0c03548>.
15
16 (37) Canaria, C. A.; So, J.; Maloney, J. R.; Yu, C. J.; Smith, J. O.; Roukes, M. L.; Fraser, S. E.;
17 Lansford, R. Formation and Removal of Alkylthiolate Self-Assembled Monolayers on Gold in
18 Aqueous Solutions. *Lab. Chip* **2006**, *6* (2), 289. <https://doi.org/10.1039/b510661c>.
19
20 (38) Porter, M. D.; Bright, T. B.; Allara, D. L.; Chidsey, C. E. D. Spontaneously Organized
21 Molecular Assemblies. 4. Structural Characterization of n-Alkyl Thiol Monolayers on Gold by
22 Optical Ellipsometry, Infrared Spectroscopy, and Electrochemistry. *J. Am. Chem. Soc.* **1987**,
23 *109* (12), 3559–3568. <https://doi.org/10.1021/ja00246a011>.
24
25 (39) Liu, B.; Bard, A. J.; Mirkin, M. V.; Creager, S. E. Electron Transfer at Self-Assembled
26 Monolayers Measured by Scanning Electrochemical Microscopy. *J. Am. Chem. Soc.* **2004**,
27 *126* (5), 1485–1492. <https://doi.org/10.1021/ja038611p>.
28
29 (40) Osawa, M. Surface-Enhanced Infrared Absorption. In *Near-Field Optics and Surface*
30 *Plasmon Polaritons*; Kawata, S., Ed.; Topics in Applied Physics; Springer: Berlin, Heidelberg,
31 2001; pp 163–187. https://doi.org/10.1007/3-540-44552-8_9.
32
33 (41) Unni, B.; Burgess, I. J. Electrochemical and Surface Enhanced Infrared Absorption
34 Spectroscopy Studies of TEMPO Self-Assembled Monolayers. *Electrochimica Acta* **2021**, *381*,
35 138263. <https://doi.org/10.1016/j.electacta.2021.138263>.
36
37 (42) Feng, Y.; Dionne, E. R.; Toader, V.; Beaudoin, G.; Badia, A. Odd–Even Effects in
38 Electroactive Self-Assembled Monolayers Investigated by Electrochemical Surface Plasmon
39 Resonance and Impedance Spectroscopy. *J. Phys. Chem. C* **2017**, *121* (44), 24626–24640.
40 <https://doi.org/10.1021/acs.jpcc.7b08053>.
41
42 (43) Shan, X.; Patel, U.; Wang, S.; Iglesias, R.; Tao, N. Imaging Local Electrochemical Current
43 via Surface Plasmon Resonance. *Science* **2010**, *327* (5971), 1363–1366.
44 <https://doi.org/10.1126/science.1186476>.
45
46 (44) Sawaguchi, T.; Mizutani, F.; Yoshimoto, S.; Taniguchi, I. Voltammetric and in Situ STM
47 Studies on Self-Assembled Monolayers of 4-Mercaptopyridine, 2-Mercaptopyridine and
48 Thiophenol on Au(111) Electrodes. *Electrochimica Acta* **2000**, *45* (18), 2861–2867.
49 [https://doi.org/10.1016/S0013-4686\(00\)00360-1](https://doi.org/10.1016/S0013-4686(00)00360-1).
50
51
52
53
54
55
56
57
58
59
60

- 1
2
3
4
5
6
7
8
9
10
11
12
13
14
15
16
17
18
19
20
21
22
23
24
25
26
27
28
29
30
31
32
33
34
35
36
37
38
39
40
41
42
43
44
45
46
47
48
49
50
51
52
53
54
55
56
57
58
59
60
- (45) Zhou; Baunach, T.; Ivanova, V.; Kolb, D. M. Structure and Electrochemistry of 4,4'-Dithiodipyridine Self-Assembled Monolayers in Comparison with 4-Mercaptopyridine Self-Assembled Monolayers on Au(111). *Langmuir* **2004**, *20* (11), 4590–4595. <https://doi.org/10.1021/la049903m>.
- (46) Herrera, S.; Tasca, F.; Williams, F. J.; Calvo, E. J.; Carro, P.; Salvarezza, R. C. Surface Structure of 4-Mercaptopyridine on Au(111): A New Dense Phase. *Langmuir* **2017**, *33* (38), 9565–9572. <https://doi.org/10.1021/acs.langmuir.7b01627>.
- (47) Silva, J. F.; Pavez, J.; Silva, C. P.; Zagal, J. H. Electrocatalytic Activity of Modified Gold Electrodes Based on Self-Assembled Monolayers of 4-Mercaptopyridine and 4-Aminothiophenol on Au(111) Surfaces Chemically Functionalized with Substituted and Unsubstituted Iron Phthalocyanines. *Electrochimica Acta* **2013**, *114*, 7–13. <https://doi.org/10.1016/j.electacta.2013.10.017>.
- (48) Karthik, N.; Asha, S.; Sethuraman, M. G. Influence of pH-Sensitive 4-Aminothiophenol on the Copper Corrosion Inhibition of Hybrid Sol–Gel Monolayers. *J. Sol-Gel Sci. Technol.* **2016**, *78* (2), 248–257. <https://doi.org/10.1007/s10971-015-3944-5>.
- (49) Hayes, W. A.; Shannon, C. Electrochemistry of Surface-Confined Mixed Monolayers of 4-Aminothiophenol and Thiophenol on Au. *Langmuir* **1996**, *12* (15), 3688–3694. <https://doi.org/10.1021/la9507390>.
- (50) Raj, C. R.; Kitamura, F.; Ohsaka, T. Electrochemical and in Situ FTIR Spectroscopic Investigation on the Electrochemical Transformation of 4-Aminothiophenol on a Gold Electrode in Neutral Solution. *Langmuir* **2001**, *17* (23), 7378–7386. <https://doi.org/10.1021/la010746q>.
- (51) Dong, L.; Yang, X.; Zhang, C.; Cerjan, B.; Zhou, L.; Tseng, M. L.; Zhang, Y.; Alabastri, A.; Nordlander, P.; Halas, N. J. Nanogapped Au Antennas for Ultrasensitive Surface-Enhanced Infrared Absorption Spectroscopy. *Nano Lett.* **2017**, *17* (9), 5768–5774. <https://doi.org/10.1021/acs.nanolett.7b02736>.
- (52) Zhao, L.-B.; Chen, J.-L.; Zhang, M.; Wu, D.-Y.; Tian, Z.-Q. Theoretical Study on Electroreduction of P-Nitrothiophenol on Silver and Gold Electrode Surfaces. *J. Phys. Chem. C* **2015**, *119* (9), 4949–4958. <https://doi.org/10.1021/jp512957c>.
- (53) Zhang, Z.; Imae, T. Study of Surface-Enhanced Infrared Spectroscopy: 1. Dependence of the Enhancement on Thickness of Metal Island Films and Structure of Chemisorbed Molecules. *J. Colloid Interface Sci.* **2001**, *233* (1), 99–106. <https://doi.org/10.1006/jcis.2000.7220>.
- (54) Baillieul, M.; Rinnert, E.; Lemaitre, J.; Michel, K.; Colas, F.; Bodiou, L.; Demésy, G.; Kakuta, S.; Rumyantseva, A.; Lerondel, G.; Boukerma, K.; Renversez, G.; Toury, T.; Charrier, J.; Nazabal, V. Surface Functionalization with Polymer Membrane or SEIRA Interface to

1
2
3 Improve the Sensitivity of Chalcogenide-Based Infrared Sensors Dedicated to the Detection
4 of Organic Molecules. *ACS Omega* **2022**, 7 (51), 47840–47850.
5 <https://doi.org/10.1021/acsomega.2c05502>.
6
7

- 8 (55) Verger, F.; Pain, T.; Nazabal, V.; Boussard-Plédel, C.; Bureau, B.; Colas, F.; Rinnert, E.;
9 Boukerma, K.; Compère, C.; Guilloux-Viry, M.; Deputier, S.; Perrin, A.; Guin, J. P. Surface
10 Enhanced Infrared Absorption (SEIRA) Spectroscopy Using Gold Nanoparticles on As₂S₃
11 Glass. *Sens. Actuators B Chem.* **2012**, 175, 142–148.
12 <https://doi.org/10.1016/j.snb.2012.01.038>.
13
14
- 15 (56) Shervedani, R. K.; Hatefi-Mehrjardi, A.; Babadi, M. K. Comparative Electrochemical Study
16 of Self-Assembled Monolayers of 2-Mercaptobenzoxazole, 2-Mercaptobenzothiazole, and
17 2-Mercaptobenzimidazole Formed on Polycrystalline Gold Electrode. *Electrochimica Acta*
18 **2007**, 52 (24), 7051–7060. <https://doi.org/10.1016/j.electacta.2007.05.030>.
19
20
- 21 (57) Bharathi, S.; Yegnaraman, V.; Rao, G. P. Potential-Dependent “Opening” and “Closing” of
22 Self-Assembled 2-Mercaptobenzthiazole on Gold Substrates. *Langmuir* **1993**, 9 (7), 1614–
23 1617. <https://doi.org/10.1021/la00031a002>.
24
25
- 26 (58) Sandhyarani, N.; Skanth, G.; Berchmans, S.; Yegnaraman, V.; Pradeep, T. A Combined
27 Surface-Enhanced Raman–X-Ray Photoelectron Spectroscopic Study of 2-
28 Mercaptobenzothiazole Monolayers on Polycrystalline Au and Ag Films. *J. Colloid Interface*
29 *Sci.* **1999**, 209 (1), 154–161. <https://doi.org/10.1006/jcis.1998.5882>.
30
31
- 32 (59) Morhart, T. A.; Unni, B.; Lardner, M. J.; Burgess, I. J. Electrochemical ATR-SEIRAS Using
33 Low-Cost, Micromachined Si Wafers. *Anal. Chem.* **2017**, 89 (21), 11818–11824.
34 <https://doi.org/10.1021/acs.analchem.7b03509>.
35
36
- 37 (60) Siddiqui, A.-R.; N’Diaye, J.; Martin, K.; Baby, A.; Dawlaty, J.; Augustyn, V.; Rodríguez-
38 López, J. Monitoring SEIRAS on a Graphitic Electrode for Surface-Sensitive Electrochemistry:
39 Real-Time Electrografting. *Anal. Chem.* **2024**.
40 <https://doi.org/10.1021/acs.analchem.3c04407>.
41
42
- 43 (61) de Carvalho, F. A.; Resende, A.; Leão, V. A. Gold Leaching by Sodium Chloride and
44 Calcium Hypochlorite Solutions. In *Extraction 2018*; Davis, B. R., Moats, M. S., Wang, S.,
45 Gregurek, D., Kapusta, J., Battle, T. P., Schlesinger, M. E., Alvear Flores, G. R., Jak, E.,
46 Goodall, G., Free, M. L., Asselin, E., Chagnes, A., Dreisinger, D., Jeffrey, M., Lee, J., Miller, G.,
47 Petersen, J., Ciminelli, V. S. T., Xu, Q., Molnar, R., Adams, J., Liu, W., Verbaan, N., Goode, J.,
48 London, I. M., Azimi, G., Forstner, A., Kappes, R., Bhambhani, T., Eds.; The Minerals, Metals
49 & Materials Series; Springer International Publishing: Cham, 2018; pp 1787–1796.
50 https://doi.org/10.1007/978-3-319-95022-8_148.
51
52
- 53 (62) Cuesta, A. ATR-SEIRAS for Time-Resolved Studies of Electrode–Electrolyte Interfaces.
54 *Curr. Opin. Electrochem.* **2022**, 35, 101041. <https://doi.org/10.1016/j.coelec.2022.101041>.
55
56
57
58
59
60

- 1
2
3 (63) Girard, H. A.; Petit, T.; Perruchas, S.; Gacoin, T.; Gesset, C.; Arnault, J. C.; Bergonzo, P.
4 Surface Properties of Hydrogenated Nanodiamonds: A Chemical Investigation. *Phys. Chem.*
5 *Chem. Phys.* **2011**, *13* (24), 11517–11523. <https://doi.org/10.1039/C1CP20424F>.
6
7
8 (64) Farquhar, A. K.; Dykstra, H. M.; Waterland, M. R.; Downard, A. J.; Brooksby, P. A.
9 Spontaneous Modification of Free-Floating Few-Layer Graphene by Aryldiazonium Ions:
10 Electrochemistry, Atomic Force Microscopy, and Infrared Spectroscopy from Grafted Films.
11 *J. Phys. Chem. C* **2016**, *120* (14), 7543–7552. <https://doi.org/10.1021/acs.jpcc.5b11279>.
12
13
14 (65) Hadj, F. A. E.; Amiar, A.; Cherkaoui, M.; Chazalviel, J.-N.; Ozanam, F. Study of Organic
15 Grafting of the Silicon Surface from 4-Nitrobenzene Diazonium Tetrafluoroborate.
16 *Electrochimica Acta* **2012**, *70*, 318–324. <https://doi.org/10.1016/j.electacta.2012.03.072>.
17
18
19 (66) Wong, E. H. J.; May, G. L.; Wilde, C. P. Oxidative Desorption of Thiols as a Route to
20 Controlled Formation of Binary Self Assembled Monolayer Surfaces. *Electrochimica Acta*
21 **2013**, *109*, 67–74. <https://doi.org/10.1016/j.electacta.2013.07.072>.
22
23
24 (67) Gong, K.; Fang, Q.; Gu, S.; Li, S. F. Y.; Yan, Y. Nonaqueous Redox-Flow Batteries: Organic
25 Solvents, Supporting Electrolytes, and Redox Pairs. *Energy Environ. Sci.* **2015**, *8* (12), 3515–
26 3530. <https://doi.org/10.1039/C5EE02341F>.
27
28
29 (68) Snyder, L. R. Classification of the Solvent Properties of Common Liquids. *J. Chromatogr.*
30 *Sci.* **1978**, *16* (6), 223–234. <https://doi.org/10.1093/chromsci/16.6.223>.
31
32
33 (69) Darwish, N.; Eggers, P. K.; Ciampi, S.; Zhang, Y.; Tong, Y.; Ye, S.; Paddon-Row, M. N.;
34 Gooding, J. J. Reversible Potential-Induced Structural Changes of Alkanethiol Monolayers on
35 Gold Surfaces. *Electrochem. Commun.* **2011**, *13* (5), 387–390.
36 <https://doi.org/10.1016/j.elecom.2011.01.025>.
37
38
39 (70) Reinsberg, P. H.; Baltruschat, H. Potential- and Cation-Dependent Adsorption of
40 Acetonitrile on Gold Investigated via Surface Enhanced Infrared Absorption Spectroscopy.
41 *Electrochimica Acta* **2020**, *334*, 135609. <https://doi.org/10.1016/j.electacta.2019.135609>.
42
43
44 (71) Solomun, T.; Christmann, K.; Baumgaertel, H. Interaction of Acetonitrile and Benzonitrile
45 with the Gold (100) Surface. *J. Phys. Chem.* **1989**, *93* (20), 7199–7208.
46 <https://doi.org/10.1021/j100357a035>.
47
48
49
50
51
52
53
54
55
56
57
58
59
60